Voltage control of magnetic hysteresis in a nickel nanoparticle

P. Gartland, W. Jiang, and D. Davidović

Phys. Rev. B **91**, 235408 — Published 8 June 2015

DOI: 10.1103/PhysRevB.91.235408

Voltage Control of Magnetic Hysteresis in a Nickel Nanoparticle

P. Gartland,[1,*] W. Jiang,[1] and D. Davidović[1]

[1]*School of Physics, Georgia Institute of Technology, Atlanta, GA 30332*

(Dated: May 15, 2015)

Abstract

The effects of voltage bias on magnetic hysteresis in single Ni particles 2-3nm in diameter are measured between temperatures of 60mK and 4.2K, using sequential electron tunneling through the particle. While some Ni particles do not display magnetic hysteresis in tunneling current versus magnetic field, in the Ni particles that display hysteresis, the effect of bias voltage on magnetic switching field is nonlinear. The magnetic switching field changes weakly in voltage interval ∼1mV above the tunneling onset voltage, and rapidly decreases versus voltage above that interval. A voltage-driven mechanism explaining this nonlinear suppression of magnetic hysteresis is presented, where the key effect is a magnetization blockade due to the addition of spin-orbit anisotropy ϵ_{so} to the particle by a single electron. A necessary condition for the particle to exhibit magnetization blockade is that ϵ_{so} increases when the magnetization is slightly displaced from the easy axis. In that case, an electron will be energetically unable to access the particle if the magnetization is sufficiently displaced from the easy axis, which leads to a voltage interval where magnetic hysteresis is possible that is comparable to ϵ_{so}/e, where e is the electronic charge. If ϵ_{so} decreases vs magnetization displacement from the easy axis, there is no magnetization blockade and no hysteresis.

PACS numbers: 73.23.Hk,73.63.Kv,73.50.-h

I. INTRODUCTION

The loss of magnetic hysteresis in nanomagnets arises due to the irreversible coupling of a magnetic sample to its environment, and is well understood in the case of thermal equilibrium[1–3]. In this article, we address the loss of magnetic hysteresis in the case of a voltage-biased nanomagnet. Such a nanomagnet is attached to electric leads via two high resistance tunneling junctions, and the electron transport through the nanomagnet at low temperatures exhibits Coulomb blockade and sequential electron tunneling. Prior measurements of voltage biased single magnetic molecules, in a double tunneling barrier device, showed no magnetic hysteresis, even at temperatures much lower than the blocking temperature.[4,5] In contrast, bulk measurements in ensembles of such molecules show hysteresis at low temperature[6,7]. Recent scanning tunneling microscopy experiments show that antiferromagnetic and ferromagnetic spin chains of only a few atoms can display hysteresis, though the lifetimes of ferromagnetically stable states are much shorter[8,9]. In single Co particles a few nm in diameter, in a double tunnel barrier device, electron transport measurements find hysteresis[10–12]. In this article we find that voltage-biased single Ni particles 2-3nm in diameter lie at the threshold of stable magnetic hysteresis. While some of our Ni particle samples do not display magnetic hysteresis at low temperature and low bias voltage, other Ni particle samples display hysteresis in current versus magnetic field. In the latter case, we find that the magnetic switching field is initially weakly dependent on bias voltage. But at voltages $\sim$1mV above the voltage threshold for sequential electron tunneling, the magnetic switching field quickly diminishes with further increase in bias voltage, and the signatures of magnetic hysteresis are quickly lost. This property is explained in this article in terms of bias voltage control of magnetic hysteresis. The possibility of bias voltage-control of magnetization dynamics in a voltage-biased ferromagnetic nanoparticle was first proposed by Waintal and Brouwer.[13] In their proposal, the magnetization relaxation time is tunable by the bias voltage and temperature. Their model has limited scope, however, because the spin-orbit (so) interaction is taken into account only trivially, by the simple uniaxial magnetic anisotropy energy of the particle. The effects of so-shifts (ϵ_{so}) of discrete energy levels were not considered. Since ϵ_{so} in transition metal particles ($\sim$ 1meV) is much larger than the magnetic anisotropy energy (per spin, $\sim$ 0.01meV),[10,11,14] the model does not apply to realistic transition metal ferromagnetic particles. In this work, we extend the model from

Ref. 13 to include the spin-orbit shifts of discrete levels, and find that the extended model explains our results well. We find that the necessary condition for magnetic hysteresis is that ϵ_{so} increases in response to magnetization movement from the easy axis, due to an effective magnetization blockade. If the condition is satisfied, the voltage scale governed by ϵ_{so} determines the bias voltage range where hysteresis can be detected. If ϵ_{so} decreases in response to magnetization displacement from the easy axis, then magnetic hysteresis will be unstable with respect to sequential electron tunneling.

The outline of this article is as follows. In section II, we describe the measurements of magnetization dynamics as a function of temperature and bias voltage, and the differential conductance spectra characteristics. In section III, we introduce the basic theory and numerical models to explain the main effects observed in section II. In section IV, we describe the detailed theory behind our observation of an effective magnetization blockade induced by voltage control of hysteresis. Finally, in section V, we summarize our main results and point to future research areas.

II. EXPERIMENTAL METHODS

As shown in Fig. 1-A and 1-B, our samples consist of one or few Ni particles immersed between two Al leads in a high-resistance aluminum-oxide double tunnel junction. The sample fabrication process has been described in our earlier work[12], and additional details are given in appendix A. Fig. 1-B shows the image of Ni particles created by the fabrication process. The $I(V)$ curve of a Ni sample at $T = 0.06$K and an applied magnetic field of $B = 0.5$T is displayed Fig. 1-C. The sample exhibits clear Coulomb blockade, which is the low voltage region where the current is negligibly weak.

To determine if the particle has magnetic hysteresis, a magnetic field is applied parallel to the film plane. The bias voltage and temperature are held fixed, and the current is observed while sweeping the magnetic field slowly, at low temperatures.

We study the effects of magnetization dynamics in the Ni particle by measuring the following quantities: (1) temperature dependence of the magnetic switching field at fixed bias voltage, (2) bias voltage dependence of the magnetic switching field at fixed temperature, and (3) tunneling spectra and current noise versus magnetic field. Five Ni particle samples from the same sample fabrication batch have been studied, and are mounted in the dilution

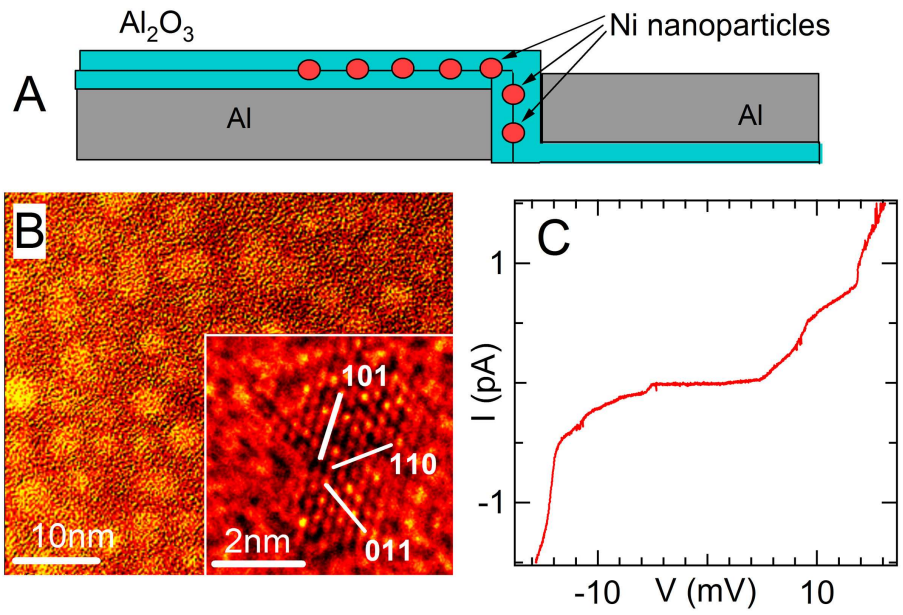

FIG. 1. Experimental arrangement of tunneling through single Ni particles. (A) Double barrier tunneling geometry. (B) Transmission Electron Micrograph of Ni particles on amorphous Al_2O_3 background. Inset: zoomed figure that displays crystal facet of Ni particle. (C) Current (I) vs. voltage (V) curve at $B = 0.5$T and $T = 0.06$K.

refrigerator at the same time. Only two of the five samples display magnetic hysteresis in tunneling current versus magnetic field at low temperature and bias voltage, while the remaining three samples show no detectable hysteresis at 0.06K temperature, for any bias voltage. For the presentation in this paper, we select a representative sample that displayed magnetic hysteresis at low temperatures and bias voltage. The samples displaying no magnetic hysteresis will be discussed in a separate publication. The second sample that exhibits magnetic hysteresis reproduces the key observations from Ni sample 1.

A. Temperature Dependence of the Switching Field

First, we study the hysteresis of the tunneling current vs. magnetic field, as a function of temperature at fixed bias voltage.

Figs. 2-A and 2-B display hysteresis loops in current versus magnetic field, at $T = 1.5$K and $T = 0.06$K, respectively, at a bias of 7.8mV.[15] There is pronounced current noise, in

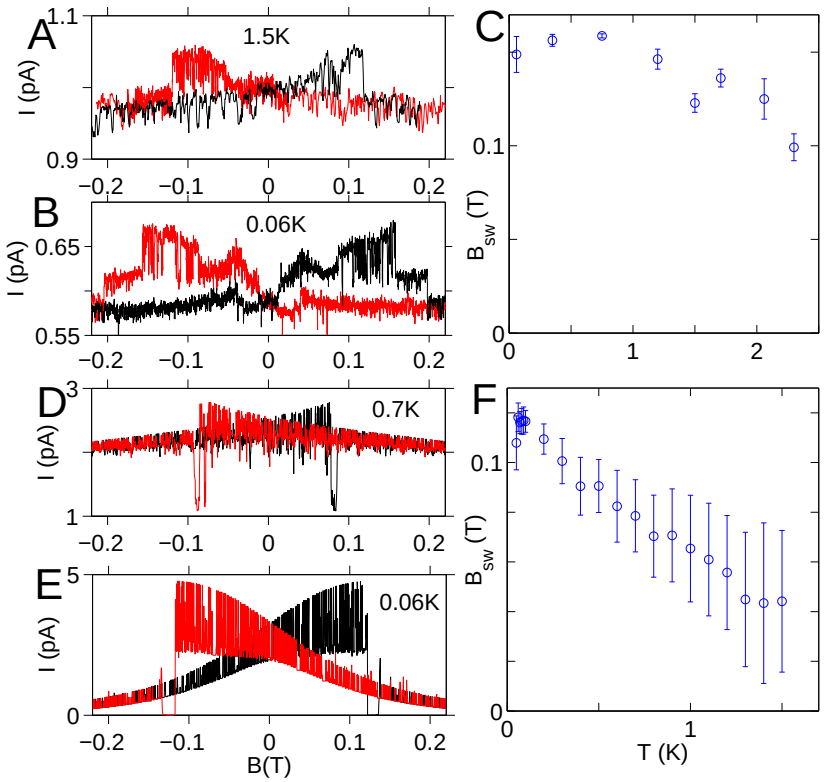

FIG. 2. Hysteresis loops in current versus magnetic field and temperature dependence of switching fields. (A),(B) Representative measured hysteresis loops of the Ni sample. Red (Black) curves corresponds to decreasing (increasing) magnetic field sweep direction. (C) Temperature dependence of the switching field averaged over 10 sweeps of magnetic field. (D),(E) Simulated hysteresis loops at different temperatures. (F) Simulated switching field vs. temperature as taken over 50 simulation runs. Error bar indicate ± standard deviation.

the form of downward spikes in current. After such a spike, current generally returns back to the value before the spike. The magnetic field locations of the spikes are random and not reproducible between repeated field sweeps, so the spikes represent noise. In addition to the noise, however, one can see that the current switches between two different values in the vicinity of ± 0.12T at $T = 1.5$K and ± 0.16T at $T = 0.06$K in Fig. 2-A and 2-B, respectively. Those switches are reproducible between different sweeps, with the standard deviation of the switching field shown by the error bars in Fig. 2-C. Similar to the work in Refs. 10–12, the switching fields as measured from the current switches will be identified here as the magnetic switching fields of the Ni particle. Fig. 2-B shows the temperature dependence

of the switching field at 7.8mV. At each temperature, 10 magnetic hysteresis loops are measured, to obtain the average switching field. The largest temperature where magnetic hysteresis is resolved is 2.3K. Above that temperature, there is a loss of magnetoresistance contrast at the expected switching field. The extrapolated temperature where the switching field goes to zero (similar to the blocking temperature T_B) is $\sim 4-5$K. In comparison, in previously studied similarly sized Co particles, which had magnetic hysteresis at 4.2K, the extrapolated temperature for the suppression of magnetic hysteresis was ≈ 12K.[12] The blocking temperature in our Ni nanoparticle is comparable to that of a magnetic molecule Mn-12[16]. Figs. 2-D,2-E, and 2-F display numerical simulations that will be discussed in the theory section of the paper. In that section, we will estimate the size of the particle and find a diameter ≈2-3nm. We note that the measured switching field versus decreasing temperature saturates at ~ 1K.

B. Hysteresis dependence on voltage bias

Next, we discuss our measurements of the current versus magnetic field at $T = 0.06$K, as a function of the bias voltage applied across the particle, and discuss the main result of the paper. Fig. 3-A displays the experimental data in the form of single sweeps of current vs. a decreasing magnetic field, for different bias voltage values. Fig. 3-B contains line profiles taken from individual constant-bias sections of Fig. 3-A. The line profiles are offset by 0.08pA for clarity. One notable feature in Fig. 3-A and 3-B is the symmetric positive peak in current versus field, of width ~ 30mT centered at 0T. the peak is an artifact arising from the field reversal in the superconducting magnet. The artifact disappears when the sweep rate is sufficiently but impractically reduced, and thus will not be discussed further.

The magnetic switching fields are marked by arrows in Fig. 3-A and 3-B. Our main result is that the magnetic switching field is weakly dependent on voltage in the interval $6.5-9$mV, and drops rapidly between 9 and 10mV, while above 10mV, there is a loss of magnetoresistance contrast at the anticipated switching field. At low voltages, below the onset of tunneling current, there is also a loss of magnetoresistance contrast at the switching field because the current is too small to be resolved. The tunneling current increases relatively quickly in the voltage interval $6.5-9$mV, where the switching field is constant (that is, $\Delta I_1 \approx 0.4$pA over this bias range). However, the current is only weakly chang-

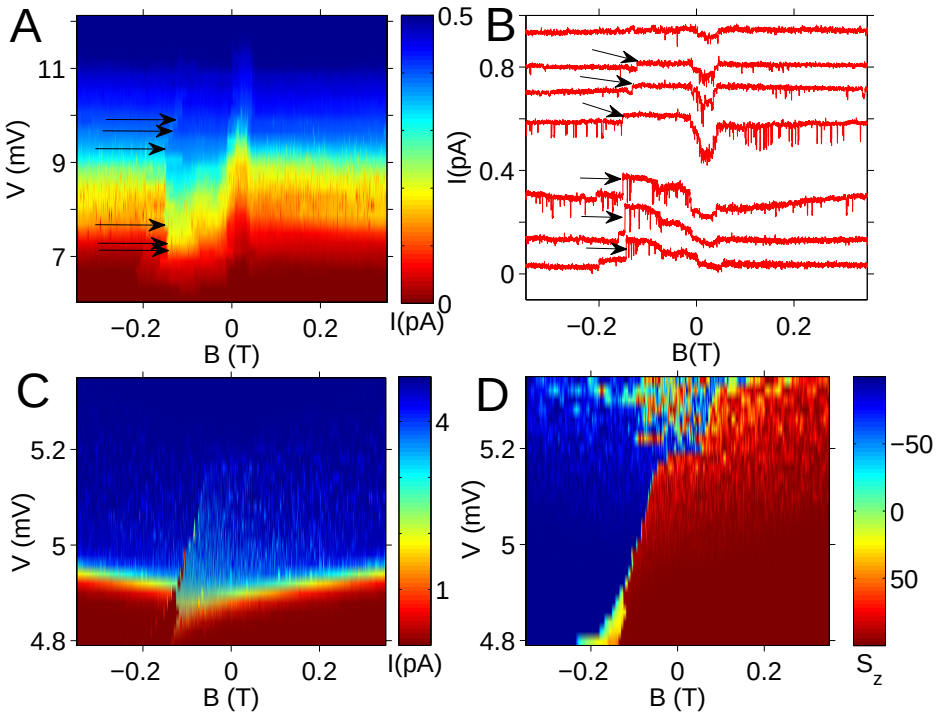

FIG. 3. Colorscale plots of dependence of hysteresis on the applied bias voltage. In all cases, magnetic field is only swept from right to left. Black arrows correspond to magnetic switching events. (A) Experimental data of hysteresis in current as a function of magnetic bias voltage V. (B) Data slices at constant voltage values of 7.1,7.3,7.7,9.3,9.7,9.9, and 10.7 mV, taken from colorplot in (A). Each slice is offset vertically by 0.08pA for visual clarity. (C) Simulation of hysteresis of particle current as a function of V. (D) Simulation of hysteresis of particle magnetization projection on z-axis as a function of V.

ing over the narrow voltage regime where the magnetic switching field is reduced (that is, $\Delta I_2 \approx 0.05$pA). So, it can be concluded that the magnetic hysteresis suppression is bias-voltage driven, rather than proportional to the tunneling current as in our previous work[12]. In the power range $(0, 3.6)$fW the switching field is nearly constant, while it takes only an additional 0.5fW to suppress the switching field above 9mV. This shows that the effect is not due to simple heating, which would be proportional to the power. Further evidence that heating is not responsible for the suppression of magnetic hysteresis is supplied by the width of the spectral levels in high field, and will be discussed in the next section. Additional data

on bias voltage dependence of magnetic switching field, over a wider voltage range than here, are provided in appendix C.

C. Tunneling Spectra

In a voltage biased quantum dot, the differential conductance (dI/dV) versus bias voltage at low temperature is known as the tunneling spectra, due to the fact that the differential conductance peaks map to quantum levels of the particle. At voltages corresponding to such peaks, the Fermi level in one of the leads is equal to the energy difference between the final and the initial quantum state of the particle, after and before a single electron tunneling event, respectively. In our Ni particles, while magnetic field sweeps at fixed voltage bias display both current noise in the form of spikes, and reproducible magnetic switching at low voltage, as already discussed, the tunneling spectra for a given sample possess a higher complexity. In the measurement of the tunneling spectra vs magnetic field, the magnetic field sweeps slowly while the bias voltage sweeps more quickly.[17] The current noise leads to strong noise in differential conductance, making identification of the magnetic switching field in the tunneling spectra difficult. A further complication is that the spectra may not display hysteresis as a function of magnetic field; that is, the presence of hysteresis vs. magnetic field in a given conductance spectra is dependent on the voltage range where the spectra is measured.

Fig. 5A displays the tunneling spectra of Ni sample 1 in a voltage interval $4 - 12$ mV and a magnetic field interval of ± 11.5T. The noise in differential conductance is manifested as apparent speckle noise over the large voltage bandwidth in the low magnetic field region. However, in the higher field regime, the noise is reduced as the spectral width of the lowest level sharpens into two linear functions of field. This is shown in Fig. 5-B and 5-C, which show data slices of Ni sample 1 at $B = 0.17$T and $B = 11.3$T, respectively, taken from Fig. 5-A. In Fig. 5-B, over wide voltage bandwidth, the differential conductance exhibits noise and rapidly oscillating values, while in Fig. 5-C, the noise is much less pronounced. Rather, the spectra have collapsed into a smaller voltage range.

The full width-half maximum (FWHM) of the lowest conductance peak can be obtained by fitting the conductance peak to a Gaussian function, which is indicated by full line in Fig. 5C. The fit leads to a FWHM of 220μeV. The FWHM can be related to the electron

temperature T_e in the leads as $k_B T_e < FWHM/3.5(1 + c_1/c_2) = FWHM/7.7$, leading to electron temperature of approximately 0.3K. Here, $c_1/c_2 \approx 1.2$ is the capacitance ratio obtained from the ratio of the current onset voltage at positive and negative bias, and 3.5 is from the FWHM of the derivative of the Fermi function. Since the electron temperature is much smaller than the temperature below which the switching field saturates (see Fig. 2), it confirms that sample heating cannot be responsible for the bias voltage dependence of the switching field.

Fig. 5-D,E,F display the numerically simulated spectra, showing qualitative agreement with the magnetic field dependence of the observed conductance speckle noise and bandwidth. This will be further discussed in the theory section of the paper.

III. MODELING USING MASTER EQUATIONS

We model the physics of electron transport through Ni particles using two magnetic Hamiltonians, and assume that the particle is in the sequential electron tunneling regime, wherein the electron number on the particle alternates between N and $N+1$. The particle magnetic Hamiltonian therefore alternates between H_0 and H_1, where $H_0 = -KS_z^2/S_0 + 2\mu_B B S_z$ and $H_1 = H_0 + \epsilon \left[\cos\theta_{SE} S_z + \sin\theta_{SE} S_x\right]^2 / S_0^2 + \epsilon_z S_z^2/S_0^2 + E_0$. where B is the magnetic field. S_0 is the ground state spin of the N-electron particle, in units of $\hbar$. For the sake of notational simplification, we have not written explicitly that S_0 changes by 1/2 upon the electron tunneling event[18]. The extra terms in H_1 correspond to the anisotropy added by a single electron. To motivate this form of the single electron anisotropy, we note that the discrete electron-box levels in a transition metal ferromagnetic particle are anisotropic with respect to the direction of the total magnetization, and they fluctuate on the order of $\epsilon_{so} = \hbar/\tau_{so} \approx 1$meV due to the so-interaction.[14,19] Here τ_{so} is the so-flip time and is estimated to be 0.58 ps for Ni particles of this size.[14] Therefore, upon the addition of a tunneling electron onto a discrete level of the particle, an anisotropy energy shift ϵ_{so} (which is played by the role of ϵ and ϵ_z) will be added to the particle Hamiltonian. Such so-shifts in a ferromagnetic nanoparticle were first studied experimentally by Deshmukh *et al.*[11] We explored a parameter space of 24 different H_1 operators by varying θ_{SE}, ϵ, and ϵ_z. In each case, we obtain the eigenenergies for the $N+1$ and the N electron particle $E_{N+1,\alpha}$ and E_{N,S_z}, for the eigenstates $|N+1,\alpha\rangle$ and $|N,S_z\rangle$, respectively. We also add a constant energy term

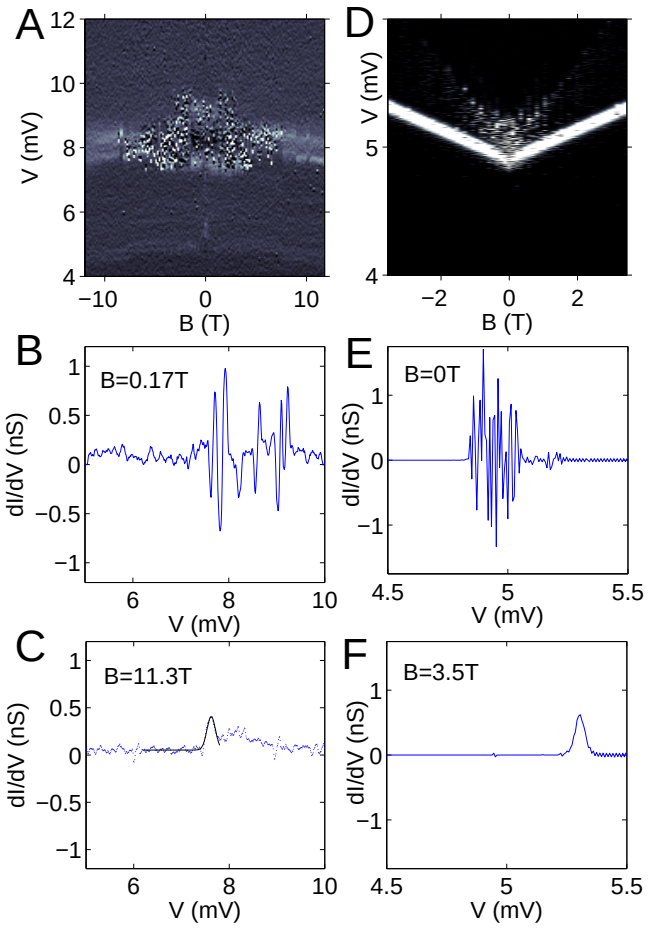

FIG. 4. Differential conductance spectra (dI/dV vs. V). (A)Experimental data of differential conductance spectra. The gray-scale range is between -0.1 nS (dark) and 0.8 nS (light). (B) and (C) display display the line profiles in conductance taken from $B = 0.17$T and $B = 11.3$T, respectively. The offset smaller curve in (C) is a local Gaussian fit to the level. (D) Simulations of the differential conductance spectra given by the main Hamiltonian considered in this paper. (E) and (F) display simulated $dI/d(V)$ curves at zero and 3.5 Tesla, respectively, taken from the gray scale in (C).

$E_0 = 2.5$meV to the $N + 1$ electron particle Hamiltonian, which accounts for the charging and the orbital energy contributions in a tunneling transition. We convert from energy to voltage using capacitive division between source and drain lead of $1 : 1$.

In this article, we consider a particular realization of H_1, where $S_0 = 100$, $K = 10\mu$eV, $\epsilon = 200\mu$eV, $\epsilon_z = -200\mu$eV, and $\theta_{SE} = \pi/6$, which qualitatively agrees with our measurement. Using such parameters, we simulate the time evolution of both the tunneling current through the particle, and the total magnetization of the particle, as a function of magnetic field and bias voltage. As we will show later, $S_0 \sim 200 - 300$ for our experimental particle, and $\epsilon_{so} \sim 1$meV. The reason for using spin $S_0 = 100$ in our computations is to make the simulations feasible in a reasonable time frame. Consequently, we reduced the effective ϵ_{so} in the simulation to maintain a comparable ratio of the total anisotropy (which scales with S_0), and ϵ_{so}.

When modeling the effects of electron transport on the eigenstates of the particle, a common approach uses a master equation to calculate the evolution of the ensemble probability distribution, among all eigenstates of the particle, until temporal convergence is achieved[13,20]. We will discuss such a calculation later (See appendix B for more details on the implementation process). Another, complementary method that yields simulation data with a more direct mapping to our experimental data is to calculate the magnetization and tunneling current as a function of time, assuming that the particle at each time step is in one of its eigenstates. We then calculate transition probabilities and generate a random event each time step based upon these transition probabilities in order to determine if the particle transitions to a different eigenstate for the next time step. Even with this relatively simple model, we are able to reproduce a significant number of characteristics of the experimental data, including the apparent noise in the measured current. We have confirmed that the statistical distribution histogram among different quantum states in time is the same as the ensemble distribution obtained from the solutions of the total master equation.

A. Modeling Temperature Dependence of Switching Field

As in the experiment, simulations are carried out at a fixed bias voltage. The voltage in the source lead is fixed at 4.9mV, which corresponds to the energy of tunneling current onset at the edge of the Coulomb blockade at zero applied magnetic field and the particle in the spin-ground state. The Fermi function value of 0 is assumed in the drain lead. The magnetic switching field $B_{sw}(T)$ as a function of temperature is determined from the switches (that is, largest discontinuity) as observed in both current and magnetization. The effect

of changing the particle temperature is taken into account in the simulations only through the shape of the Fermi level in the source lead. That is, the particle receives indirect temperature equilibration with the environment through the transport of electrons, rather than explicitly linking the particle to a thermal bath. Fig. 2-D and 2-E display simulated hysteresis in current for two representative values $T = 0.7$K and $T = 0.06$K, and Fig. 2-F shows the average simulated switching fields vs. temperature, with the error bar indicating $\pm$ standard deviation. The noise in the current hysteresis loop increases in magnitude as the field approaches the switching value. The results are in good qualitative agreement with our experimental data.

The blocking temperature in the simulation is ≈ 2K, approximately two times smaller than that estimated from measurements, while the magnetic switching fields near zero temperature are comparable between measurement and simulation. Since the blocking temperature generally scales with the size of the particle,[1,2] we can conclude that the measured particle is two times larger in volume than the simulated particle, or $S_0 = 200 - 300$, which corresponds to the particle diameter in the range 2-3nm, in agreement with the transmission electron micrograph in Fig. 1.

B. Modeling Bias Voltage Dependence of Switching Field

The simulated negatively-swept hysteresis curves in the colorplots of Fig. 3-C and 3-D were calculated using the same scheme as in the temperature dependent scans, but we varied the bias voltage for each sweep and held the temperature fixed at $T = 75$mK. In the simulations, we can also observe the particle magnetization directly. In Fig. 3-D, the magnetic switch is indicated by the sudden shift from red to blue, and is well-defined and slowly varying over a large voltage range. Once the bias reaches 5.16mV, the magnetic switch becomes unstable and the switching field value decreases quickly. For bias values above 5.18mV, the magnetization switches at random fields. In Fig. 3-C, the simulated tunneling current, rather than the magnetization, is displayed.

The simulation data in Fig. 5 consists of individual line profiles from the colorplots of Fig. 3-C and 3-D, plus data from the other field sweep direction. At the lower bias values in 5-A,B, the switches in current and magnetization occur at clear, reproducible values. The magnetization vs. field begins to exhibit small-amplitude noise as the field approaches

the switching field, but the amplitude of noise in the current relative to average is much higher than the corresponding relative noise in the magnetization. However, in Fig. 5-C, the current has already reached its saturated value for the higher bias voltage value, and thus the magnetization in Fig. 5-D exhibits no hysteresis, but rather, random switching events. When current becomes saturated at the highest bias values, fluctuations in current diminish, but the switches are no longer resolvable. It is precisely this high bias voltage region of current saturation where the switching of the magnetization exhibits the most noise. This is in good agreement with our experimental data in Fig. 3-A, where the switching field varies little over a large current range, but quickly falls of when the voltage is raised further, while the current noise is suppressed above that voltage.

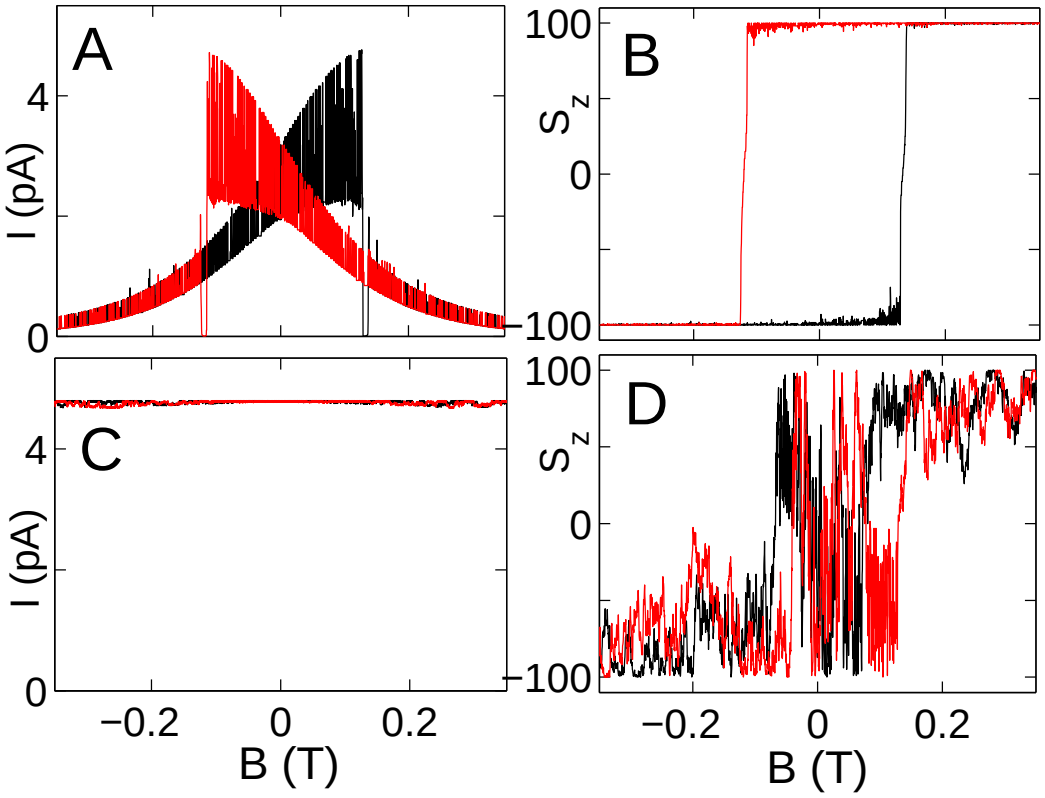

FIG. 5. Data slices taken from the simulation in Fig. 3-B,C. (A),(C) Simulated current hysteresis loops at $V = 4.90$mV and $V = 5.28$mV, respectively. (B),(D) Corresponding magnetization hysteresis loops at $V = 4.90$mV and $V = 5.28$mV, respectively. Red (black) correspond to data taken from a decreasing (increasing) field sweep.

C. Modeling Energy Spectra and Noise

The numerical simulations of the tunneling spectrum versus magnetic field are displayed by the gray scale image in Fig. 4-D. As with our measured spectra, there is significant noise in the conductance at low field in the simulation, which appears as speckle noise at low field values of the differential conductance spectra. Fig. 4-E and 4-F show data slices taken from the simulation data at $B = 0$T and $B = 3.5$T, respectively. In Fig. 4-F, the noise in conductance is reduced, and there is only a single smooth peak. This directly reproduces the qualitative structure observed in the experimental data and provides very good visual agreement; that is, there is clear noise in the spectra in the low field regions, but the noise is diminished in the high field regions. The reason for the difference in magnetic field scale between Fig. 4-A and Fig. 4-D in both bias voltage and magnetic field range again lies with the fact that our simulations used smaller spin (and therefore total anisotropy) and corresponding smaller ϵ_{so} than in the experimental case.

IV. UNDERSTANDING VOLTAGE CONTROL OF MAGNETIC HYSTERESIS

As discussed in the previous section, there is a good qualitative agreement between the observed parameters and master equation simulations. The purpose of this section is to illuminate the physics of bias voltage control. The model of voltage control of hysteresis can be understood from the perspective of an effective magnetization blockade, similar to the well known spin-blockade phenomenon studied previously in semiconducting quantum dots.[21–27] In the case of spin blockade, the tunneling current through consecutive quantum dots is diminished due to the Pauli exclusion principle. In the case of magnetization blockade, the motion of the magnetization is blocked in the neighborhood of the easy axis, due to the interplay between Coulomb blockade and the energy cost associated with deflecting the magnetization at too large an angle away from an easy axis. Consider first the case where ϵ_{so} increases as the magnetization is displaced from the easy axis. If the bias voltage is low compared with ϵ_{so}/e, then the potential energy in the leads cannot supply enough energy for the particle to transition into the excited magnetization state (that is, an electron cannot tunnel onto the particle to displace the magnetization beyond a maximum angle determined by the bias voltage), and thus the magnetization remains localized near the easy axis. Once

the bias voltage is raised past ϵ_{so}/e, however, the electron can surmount the magnetization blockade and tunnel into higher particle magnetization states. Next, consider the case where ϵ_{so} decreases as the magnetization is displaced from the easy axis. In this situation, there is no hindrance to electron transport because further displacements of the magnetization from the easy axis require decreasing amounts of energy. This runaway effect causes the magnetization to displace arbitrarily far from the easy axis as soon as the tunneling process has been initiated.

In the remainder of this section, we will explain this phenomenon of magnetization blockade in detail. In the simulations that follow, we will assume that the applied magnetic field is zero. As discussed earlier, the eigenenergies for the $N+1$ and the N electron particle are labeled $E_{N+1,\alpha}$ and E_{N,S_z}, for the eigenstates $|N+1,\alpha\rangle$ and $|N,S_z\rangle$, respectively. The values $\alpha = 0, 1, 2, ...$ are sorted in order of increasing $\langle\alpha|S_z|\alpha\rangle$. In the vicinity of the energetic minimum with negative $\langle\alpha|S_z|\alpha\rangle$, α also sorts the excited states of the $N+1$ electron particle, that is, $E_{N+1,\alpha}$ increases versus α for the Hamiltonian that we use.

We found that the tunneling density of states (DOS) is a useful structure to explain how voltage controls magnetization dynamics. For the aforementioned realization of H_0 and H_1, Fig. 6 displays the results for the tunneling density of states (DOS) for the N-electron particle with spin component S_z, where we define $DOS(S_z, E) = \sum_{\alpha} |\langle N, S_z|N+1,\alpha\rangle|^2 \delta(E_{N+1,\alpha} - E_{N,S_z} - E)$. The $\delta-$functions are broadened by convolving with a Gaussian of width 1μeV. The darkest regions correspond to zero DOS, while the white corresponds to the maximum DOS.

We simulate the single-electron-tunneling using a master equation following the procedure described in Ref. 13, to determine field and bias dependence of the converged probability distribution P_{N,S_z} and $P_{N+1,\alpha}$ of quantum states of the particle (see Appendix for more details). The source Fermi level energy of 2.45meV (or a bias voltage of 4.9mV) corresponds to the onset of tunneling at the edge of the Coulomb blockade. In this section, we discuss the bias in terms of energy rather than voltage. As mentioned previously, the conversion from voltage to energy requires capacitive division, which amounts to a factor of 2 difference between the two quantities. The Fermi function in the drain lead is set to 0 for the energy range in Fig. 6.

The white curves in the grayscale image of Fig. 6-A represent energies of various tunneling transitions between the magnetic states of the N and $N+1$ electron particle, as a function of

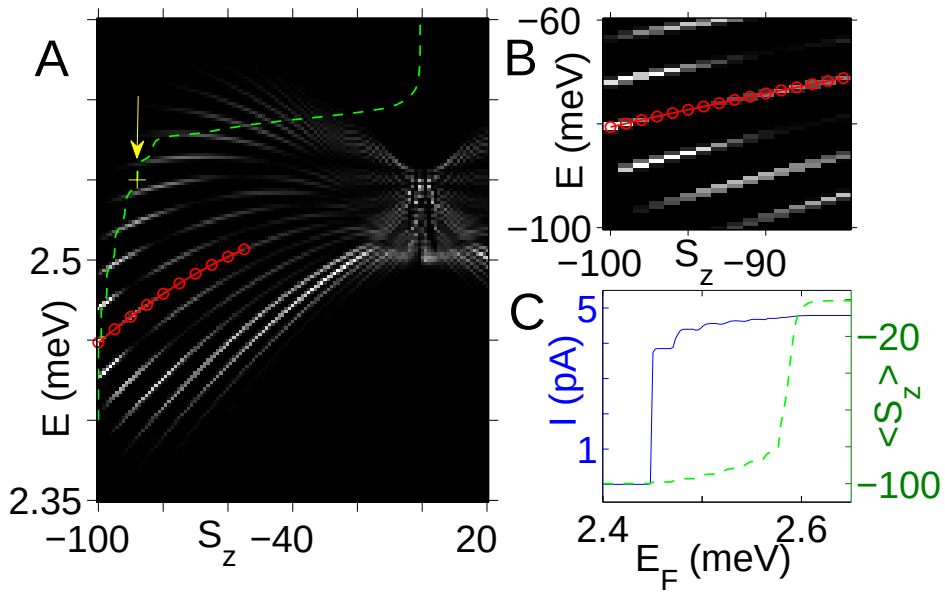

FIG. 6. Master equation simulations: (A) Tunneling density of states. Red, solid curve with circle markers corresponds to non-magnetic transitions. Green dashed curve corresponds to calculated $\langle S_z \rangle$ (bottom axis) as a function of bias E_F (left axis). (B) Zoomed region of the DOS from (A), displaying a so-shifted level increasing as a function of magnetization-displacement from easy axis. (C) Current (blue solid line) and $\langle S_z \rangle$ vs. bias E_F (green dashed line, the same as in (A)).

the initial state of the N electron particle. The distance between the curves along the y-axis is dictated by the magnon excitation energy (20μeV for this case). The tunneling transitions in the DOS span an energy range determined by ϵ_{so}, which is an order of magnitude larger than the magnon energy. Fig. 6-B shows zoomed-in DOS in the vicinity of $S_z = -S_0$. Note the transition indicated by circle markers connected with a line. At $S_z = -100$, the total DOS below the circle-marked line is zero. This indicates that, for the N-electron particle in the ground state, the tunneling transition indicated by the circle-marked line has the lowest energy, which means that after the transition the particle will be in the N+1-electron ground state. If initially $S_z = -S_0+1$, there will be only one tunneling transition with energy below the circle-marked line, which will be the transition from the first excited state of the N electron particle to the ground state of the $N+1$ electron particle. In such transition, the magnetic energy decreases. Overall, the circle-marked line indicates nonmagnetic transitions $|N, -S_0+n\rangle \rightarrow |N+1, \alpha\rangle$, where $\alpha = n$. The curves at energies above (below) the energy of the nonmagnetic transition, correspond to the magnetically exciting (relaxing) transitions,

in which $\alpha > n$ ($\alpha < n$).

In the vicinity of $S_z = -S_0$, the integral of the DOS over magnetically exciting transitions (i.e. the total weight for the transitions above the circle-marked line) is slightly higher than the integral over magnetically relaxing transitions. Consequently, if E_F in the source lead is above all tunneling transition energies, there will be a net positive energy inflow from the lead into the magnetic subsystem. Similarly, we find that the electron outflow to the drain also produces a net positive energy inflow into the magnetic subsystem. However, if E_F in the source lead is reduced to lie within the energy range spanned by the white curves, then the Fermi function in the source lead will suppress some magnetically exciting transitions. The net energy flow into the magnetic subsystem can be negative, which means that the magnetic relaxation time is finite. A similar effect was studied in Ref. 13. Due to this relaxation, a steady state value of S_z will follow.

As an example, consider the N electron particle initially in its ground state $S_z = -S_0$, and apply a bias energy of 2.55meV. Initially, for $S_z = -S_0$, all of the DOS is below E_F. Since the total probability of the magnetically exciting transitions is higher than that for the magnetically relaxing transitions, S_z will initiate a random walk in response to the applied bias, leading to S_z increasing linearly with time. A similar magnetization random walk in the absence of so-interaction was studied previously[13]. When S_z reaches ≈ -88, as shown by the yellow cross in Fig. 6-A, then a magnetically exciting transition will turn on in the DOS above E_F, as indicated by the yellow arrow in Fig. 6-A. Since this level is energetically prohibited due to the height of E_F, the magnetic energy inflow diminishes, and $\langle S_z \rangle$ will converge to slightly above $S_z = -88$. We can conclude that the required condition for the localization of S_z near the energetic minimum at $S_z = -S_0$, which is also the condition for magnetic hysteresis, is that the energy of the magnetically exciting transitions increase as S_z shifts from the ground state value. This verifies our picture of magnetization blockade, wherein the energy conservation of the tunneling process pins the magnetization within a small localized region, inducing an effective barrier against magnetization motion. The simulations produce a striking separation in the bias voltage values where the current onset occurs and where $\langle S_z \rangle$ increases to zero, as shown in Fig. 6-C. The dashed green curve in Fig. 6 is the converged $\langle S_z \rangle$ as a function of bias energy $E = E_F$, while the solid blue curve in the Fig. 6-C is the converged $I(E_F)$ curve. So, the magnitude of the current alone is not a sufficient parameter for magnetization control. Rather, it is the bias Fermi energy

that determines the control of magnetization dynamics. As we varied the parameters to study different H_1 operators, we found many Hamiltonians that would altogether prevent the possibility of magnetic hysteresis. Those H_1 operators lack magnetic levels that increase in energy as S_z shifts away from $-S_0$. This explains our numerous experimental Ni samples that showed no observable hysteresis.

V. CONCLUSIONS

In summary, we have presented an experimental realization of a bias voltage control of magnetic hysteresis in a ferromagnetic particle. Through master equation simulations and probabilistic eigenstate evolution equations, we have demonstrated the emergence of an energy scale from the spin-orbit anisotropy contribution from a single electron, which is able to explain how the range of magnetization motion is controlled by the applied bias, irrespective of the size of the tunneling current. A necessary condition for the bias voltage control of the magnetization is that the anisotropy contribution of a single electron increases in response to a small magnetization displacement from the easy axis. This constraining of magnetization motion within a localized orientation due to the energy conservation of the electron tunneling acts as an effective magnetization blockade. The qualitative results of our simulations agree remarkably well with our experimental data. In terms of spin based electronics, the next step could be to explore the use of voltage, rather than current, to control spin-transfer torque in a ferromagnetic particle or molecule, which would require spin-polarized drain and source leads.

VI. APPENDICES

A. Sample Fabrication

Samples are fabricated by using electron-beam lithography and a shadow evaporation technique. We spin-coat a bilayer of methyl methacrylate/polymethyl methacrylate (MMA/PMMA) electron-beam resist on a SiO_2 substrate. An SEM is used to define the desired sample dimensions and geometries on the substrate. Developing the samples exposes the areas of substrate exposed to the localized electron beam. Samples are placed on a rotatable stage in a vacuum chamber, which is pumped down to 10^{-7} Torr. Layers of metal

contacts and nanoparticles are evaporated in the vacuum using current-induced Joule heating of the metals. A crystal monitor is used to track the amount of metal deposited on the sample. In the first step, conducting planes of Al, 40 nm thick, are deposited, followed by 20 nm of insulating Al_2O_3 which conformally covers the conducting Al. This forms the capacitive shunt filters which divert extraneous microwave noise away from the sample electrodes. We spin-coat the samples with MMA/PMMA again and pattern the tunnel junctions. The tunnel junction consists of an Al electrode (14 nm thick) followed by a layer of insulating $Al_2O_3 \approx 1.8$ nm thick. Next a nominal thickness of 5-6 Angstroms of ferromagnetic metal are deposited, which nucleate due to surface tension and form isolated nano-islands with diameters on the order of $2-3$ nm. The lattice constant extracted from the structure in Fig. 1 of the main text confirms faced-centered-cubic Ni. In addition, energy dispersive X-ray spectra (EDS) demonstrate that the particles are made from Ni. Next, another layer of $Al_2O_3 \approx 1.8$ nm thick is deposited to form the other half of the double tunnel junction. Finally, a second conducting contact of Al (14 nm) is deposited. The remaining metal on the PMMA is washed away during a liftoff process in acetone. Samples are then wired up and attached to a dipstick to be inserted into the dilution refrigerator. The basic structure of the tunnel junction samples is as shown in Fig. 7-A, which has the capacitive ground plane beneath the tunnel junction in order to filter any unwanted high-frequency signals away from the sample. A zoomed SEM image of an exemplary device junction is displayed in Fig. 7-B.

Samples are studied in a dilution refrigerator, and the sample leads are additionally cryogenically filtered using a high loss transmission line with an exponential cut-off at frequencies ~ 10MHz. The samples sit in a Faraday cage at temperature ≈ 30mK. An on-chip filter in the form of a capacitively coupled ground plane lies beneath the sample, with a frequency cut-off also ~ 10MHz. Typical junction resistance is $\approx G\Omega$, and typical current per discrete levels is quite low, ~ 0.1pA.

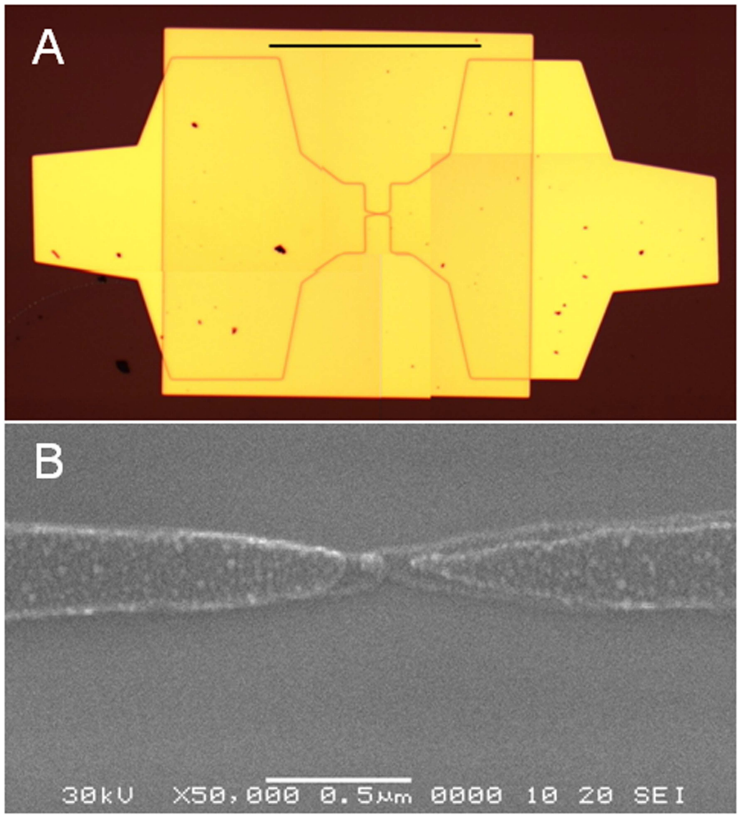

FIG. 7. (A) Optical microscope image (stitched from multiple images of the same device) of nickel tunneling device geometry with conducting ground plane beneath. The black scale bar indicates 250 microns. (B) SEM image of typical tunnel junction device. White scale bar indicates 0.5 microns.

B. Master Equation Simulations

The master equation utilized in our present work is adapted from references 20 and 13:

$$\frac{\partial P_\alpha}{\partial t} = \sum_\beta \sum_{l=L,R} \sum_{\sigma=up,down} \Gamma_{l\sigma} \Big[\left|\langle\beta|c_{\mu\sigma}|\alpha\rangle\right|^2 \left(f_l(E_\alpha - E_\beta)P_\beta - (1 - f_l(E_\alpha - E_\beta))P_\alpha\right) + \left|\langle\beta|c^\dagger_{\mu\sigma}|\alpha\rangle\right|^2 \left(-f_l(E_\beta - E_\alpha)P_\alpha + (1 - f_l(E_\beta - E_\alpha))P_\beta\right) \Big]$$

The above equation determines the evolution of the probability P_α of occupation of a given particle state $|\alpha\rangle$ in time. The spin of the electron is σ, and the tunneling rate $\Gamma_{l\sigma}$ in general could be different for the source and drain leads, and could depend on the spin polarization. The time rate of change of P_α depends on the Fermi level in the source and drain leads (L and R, respectively). These Fermi functions are evaluated at the energy differences $E_\alpha - E_\beta$ between the states involved in tunneling. Each term in the sum also depends on the overlap

between states $|\alpha\rangle$ and $|\beta\rangle$, upon the addition ($c^{\dagger}_{\mu\sigma}$) or subtraction ($c_{j\sigma}$) of an electron, where $c^{\dagger}_{\mu\sigma}$ is the electron creation operator for the μ^{th} level, and $c_{\mu\sigma}$ is the electron annihilation operator for the μ^{th} level.

While the total spin S_0 on the N-electron particles in our experiments is likely ~ 200, such calculations become very time consuming and computationally intensive, and since our goal with the master equation simulations was to derive qualitative results rather than a quantitative fit to our experimental data, we elected to do simulations with $S_0 = 100$. Additional parameters for our simulations include tunneling rate $\Gamma = 60$Mhz for both leads, time step $\Delta t = 1$ns, and total integration time $t = 25\mu$s. The probability distribution and magnetic energy are checked for saturated convergence in time.

We studied a Hamiltonian parameter space of $K = 10$, $\epsilon = [-200, 200]$, $\epsilon_z = [-200, 0, 200]$, and $\theta_{SE} = [\pi/6, \pi/4, \pi/3, \pi/2]$. All energies are in units of μeV. Due to mesoscopic fluctuations, these adjustable parameters will vary from sample to sample, and our goal was to merely sample the large possible parameter space. Note, in order to convert from E to voltage, one needs to add the orbital, the exchange, and the charging energy to E, and account for the capacitive division of the voltage. We assume there is only one quasiparticle state μ within the energy range of tunneling, and that the Fermi level in the drain is $-\infty$; that is, $f_R = 0$.

When determining the $I(V)$ characteristics, the state is initialized in the ground state of the N-electron particle. For subsequent bias voltage data points, the initial state probability distribution is taken as the saturated value from the previous voltage point. In this way, the progression of current and $\langle S_z \rangle$ will occur in the same way as in experiments.

The complementary simulation that we used in the calculation of the hysteresis loops and spectra involves the same Hamiltonian and evolution equation as used in the master equation simulations. One key difference, however, is that instead of evolving the probability distribution of all eigenstates in time simultaneously until temporal convergence, we initialize the particle in its ground state, and then calculate transition probabilities for each time step. That is, we integrate the master equation for one time step, and read all the transition probabilities in that time step. We then generate a random event according to those probabilities, leading to the new eigenstate for the particle before the next time step. For small time steps, the most likely event is that the particle will remain in the same state. We have tested this scheme for a given Hamiltonian and bias voltage, and found that the

long-time histogram of eigenstate probabilities using this method is identical to the steady state distribution of states given by the master equation, as expected.

C. Additional Hysteresis vs. Voltage Data

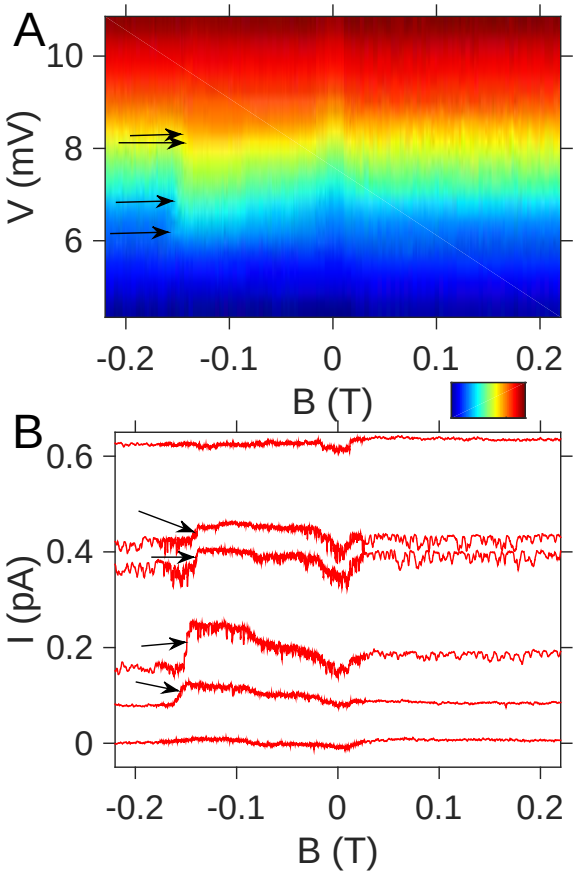

FIG. 8. Additional voltage sweep data displaying one-sided current hysteresis loops for Ni sample 1. (A) Colorplot displaying the reproducible effect of hysteresis in a specific voltage range. Blue (Red) correspond to 0pA (0.65pA). (B) Data slices taken at constant voltage values from the colorplot in (A). Curves are offset by 0.017pA for visual clarity. Black arrows indicate switching events. At the lowest and highest biases, switching resolution has been lost.

To emphasize the reproducibility of the importance of voltage bias, rather than current, on the hysteretic properties of Ni sample 1, we provide in Fig. 8-A an additional colorscale plot of current hysteresis in a narrow voltage range. Fig. 8 is an average over four voltage ramps, and the the main effect as observed in the data from Fig. 3 is reproducible. Fig. 9-B displays individual data slices from the colorplot at the following increasing voltage values: 5.4, 6.2, 6.8, 8.2, 8.4, and 10.3 mV.

Research supported by the U.S. Department of Energy, Office of Basic Energy Sciences, Division of Materials Sciences and Engineering under Award DE-FG02-06ER46281. We thank Dr. Ding from the Microscopy Center, School of Materials Science and Engineering at Georgia Institute of Technology for his help in taking the TEM image of the Ni particles.

---

* Author to whom correspondence should be addressed. E-Mail: dragomir.davidovic@physics.gatech.edu

[1] L. Néel, Ann. Géophys **5**, 99 (1949).

[2] W. F. Brown, Phys. Rev. **130**, 1677 (1963).

[3] W. Wernsdorfer, E. B. Orozco, K. Hasselbach, A. Benoit, B. Barbara, N. Demoncy, A. Loiseau, H. Pascard, and D. Mailly, Phys. Rev. Lett. **78**, 1791 (1997).

[4] E. Burzurí, A. S. Zyazin, A. Cornia, and H. S. J. van der Zant, Phys. Rev. Lett. **109**, 147203 (2012), URL `http://link.aps.org/doi/10.1103/PhysRevLett.109.147203`.

[5] M.-H. Jo, J. E. Grose, K. Baheti, M. M. Deshmukh, J. J. Sokol, E. M. Rumberger, D. N. Hendrickson, J. R. Long, H. Park, and D. C. Ralph, Nano Letters **6**, 2014 (2006).

[6] L. Thomas, F. Lionti, R. Ballou, D. Gatteschi, R. Sessoli, and B. Barbara, Nature **383**, 145 (1996).

[7] J. R. Friedman, M. P. Sarachik, J. Tejada, and R. Ziolo, Phys. Rev. Lett. **76**, 3830 (1996).

[8] S. Loth, S. Baumann, C. P. Lutz, D. M. Eigler, and A. J. Heinrich, Science **335**, 196 (2012).

[9] A. A. Khajetoorians, B. Baxevanis, C. Hbner, T. Schlenk, S. Krause, T. O. Wehling, S. Lounis, A. Lichtenstein, D. Pfannkuche, J. Wiebe, et al., Science **339**, 55 (2013), http://www.sciencemag.org/content/339/6115/55.full.pdf, URL `http://www.sciencemag.org/content/339/6115/55.abstract`.

[10] S. Gueron, M. M. Deshmukh, E. B. Myers, and D. C. Ralph, Phys. Rev. Lett. **83**, 4148 (1999).

[11] M. M. Deshmukh, S. Kleff, S. Gueron, E. Bonet, A. N. Pasupathy, J. von Delft, and D. C. Ralph, Phys. Rev. Lett **87**, 226801 (2001).

[12] W. Jiang, F. T. Birk, and D. Davidovic, Sci. Rep. **3**, 1200 (2013).

[13] X. Waintal and P. W. Brouwer, Phys. Rev. Lett. **91**, 247201 (2003).

[14] A. Cehovin, C. M. Canali, and A. H. MacDonald, Phys. Rev. B **66**, 094430 (2002).

[15] Note1, the sweep rate in Fig. 2 is 0.07T/min.In Fig. 3A, the magnetic field range $\pm$0.5T, but

the figure shows a zoomed color scale image of a scan in current versus negatively-sweeping magnetic field at rate 0.07T/min, while the bias voltage is slowly increasing from 6.0mV to 12.0mV, at a rate 0.0067mV/min. In the supplementary data in the appendix, the voltage is increased slowly from 4.5mV to 11.0mV at a rate of 0.035mV/min, while the magnetic field is swept more quickly in the interval ±0.25T at a rate 0.07T/min in the negative sweep region 0→-0.2T, and 0.28T/min elsewhere.

[16] R. Sessoli, D. Gatteschi, A. Caneschi, and M. Novak, NATURE **365**, 141 (1993), ISSN 0028-0836.

[17] Note2, for the differential conductance measurements of Fig. 4-A, the field was swept from -11.5 T to +11.5T at a rate of 41mT/minute. Simultaneously, the voltage was swept in a triangle wave from 0mV to 17.1 mV at a rate of 4.39mV/minute.

[18] Note3, this alters the spin operators, and require the use of Clebsch-Gordan coefficients upon transforming the size of the spin space. While we have included such effects in our simulations, we neglected their expression in the Hamiltonians for notational clarity.

[19] A. Cehovin, C. M. Canali, and A. H. MacDonald, Phys. Rev. B **68**, 014423 (2003).

[20] W. Jiang, P. Gartland, and D. Davidovi, Journal of Applied Physics **113**, 223703 (2013), URL `http://scitation.aip.org/content/aip/journal/jap/113/22/10.1063/1.4810853`.

[21] K. Ono, D. Austing, Y. Tokura, and S. Tarucha, SCIENCE **297**, 1313 (2002), ISSN 0036-8075.

[22] F. Koppens, J. Folk, J. Elzerman, R. Hanson, L. van Beveren, I. Vink, H. Tranitz, W. Wegscheider, L. Kouwenhoven, and L. Vandersypen, SCIENCE **309**, 1346 (2005), ISSN 0036-8075.

[23] A. K. Httel, H. Qin, A. W. Holleitner, R. H. Blick, K. Neumaier, D. Weinmann, K. Eberl, and J. P. Kotthaus, EPL (Europhysics Letters) **62**, 712 (2003), URL `http://stacks.iop.org/0295-5075/62/i=5/a=712`.

[24] A. C. Johnson, J. R. Petta, C. M. Marcus, M. P. Hanson, and A. C. Gossard, Phys. Rev. B **72**, 165308 (2005), URL `http://link.aps.org/doi/10.1103/PhysRevB.72.165308`.

[25] L. P. Rokhinson, L. J. Guo, S. Y. Chou, and D. C. Tsui, Phys. Rev. B **63**, 035321 (2001), URL `http://link.aps.org/doi/10.1103/PhysRevB.63.035321`.

[26] H. W. Liu, T. Fujisawa, Y. Ono, H. Inokawa, A. Fujiwara, K. Takashina, and Y. Hirayama, Phys. Rev. B **77**, 073310 (2008), URL `http://link.aps.org/doi/10.1103/PhysRevB.77.073310`.

[27] N. Shaji, C. Simmons, M. Thalakulam, L. J. Klein, H. Qin, H. Luo, D. Savage, M. Lagally, A. Rimberg, R. Joynt, et al., Nature Physics **4**, 540 (2008).